Journal of
Nanoscience and Nanotechnology
Vol. 5, 1552–1556, 2005

EPR Study of ZnS: Mn^{2+} Nanocrystals in Pyrex Glasses

C. X. Liu,[1] J. Y. Liu,[1] and K. Dou[2,*]

[1] *Key Laboratory of Excited State Processes, Changchun Institute of Optics, Fine Mechanics and Physics, Chinese Academy of Sciences, Changchun 130033, P. R. China*
[2] *Department of Physics, Oklahoma State University, Stillwater, OK 74078, USA*

ZnS: Mn^{2+} nanocrystals embedded in Pyrex glasses were spectrally studied using EPR and photoluminescence techniques. Photoluminescence (PL) and excitation (PLE) spectra revealed that manganese impurities can be classified as two types of luminescent centers, i.e., occupying substitutional sites $(Mn^{2+})_{sub}$ or interstitial sites $(Mn^{2+})_{int}$. Three types of manganese sites of $(Mn^{2+})_{sub}$, $(Mn^{2+})_{int}$, and Mn clusters were identified by the EPR spectra. An increase of the g_1 factor and hyperfine structure (HFS) constant with decreasing sizes of nanocrystals was observed. The increase was attributed to a hybridization of the *s-p* state of ZnS and the *d* state of manganese ions enhanced by quantum confinement effects or surface states.

Keywords: Nanocrystal, ZnS: Mn^{2+} Nanoparticle/Pyrex Glasses, EPR Spectrum.

RESEARCH ARTICLE

1. INTRODUCTION

Bulk ZnS: Mn^{2+} has been widely used as one of the most important phosphors in traditional electroluminescence materials. Much effort[1–4] has been directed towards understanding the underlying physics behind high efficiency in nanocrystals, ever since high quantum efficiency (up to 18%) and short luminescence lifetime (five orders of magnitude faster than in bulk ZnS) were reported in ZnS: Mn^{2+} nanocrystals in 1994.[1] Although preparation and optical property of glasses doped with intrinsic semiconductors or rare earth ions were extensively studied as optical materials, a number of studies on the glasses with dispersed doped semiconductor were reported,[4,5] particularly using a combination of photoluminescence (PL) and EPR techniques. In this paper, we report optical and EPR studies on ZnS: Mn^{2+} nanocrystal-doped glasses and focus on a spectral comparison between ZnS: Mn^{2+} nanocrystallites and bulk powders.

2. EXPERIMENTAL DETAILS

ZnS: Mn^{2+} nanoparticles were synthesized by using a chemical precipitation approach. Pyrex glasses (Na_2O-B_2O_3-SiO_2) dispersed with ZnS: Mn^{2+} nanocrystallites were prepared using a method as described in Ref. [4]. Na_2O-B_2O_3-SiO_2 and ZnS: Mn^{2+}(Mn^{2+}/ZnS = 1% (g/g)) powders were uniformly blended and the mixture was then heated to 1300–1500 °C for 20 minutes. The nucleation of ZnS: Mn^{2+} nanocrystallites were suppressed by rapid cooling in the environment with nitrogen gas for protection. The sizes of nanocrystal were controlled by annealing the glasses at different temperatures. The nanocrystals used for the current experiments were 3.4, 3.6 and 4.0 nm in diameter prepared by annealing glasses at 500, 550 and 600 °C, respectively. The glasses obtained were transparent and uniform, colorless or light brown. Based on the color the samples possess, we can conclude that our samples only contain Mn^{2+} ions instead of Mn^{3+}, because the glasses containing even a small amount of Mn^{3+} will give rise to a deep purple color.[5] Some parameters of the samples used for the current study are listed in Table I.

The PL and PLE spectra were measured using a Hitachi F-4000 spectrometer at room temperature. EPR measurements were performed at both room and liquid nitrogen temperature using a BRUKER ER 200D EPR spectrometer at 9.78 GHz.

3. RESULTS AND DISCUSSION

3.1. PL and PLE Spectra

A comparison of the photoluminescence (PL) and excitation (PLE) spectra of ZnS: Mn^{2+} nanocrystals/glass having

*Author to whom correspondence should be addressed.

1533-4880/2005/5/1552/005 doi:10.1166/jnn.2005.328

Table I. Experimental data of ZnS: Mn^{2+} nanocrystallites dispersed in Pyrex glasses.

	ZnS: Mn^{2+} in glass (Weight%)	Emission peak (nm)	Excitation peak (nm)	Diameter (nm)	$g_{\parallel}$	HFS | A | /$g\beta$ (mT)	A_{up}/A_{down}
N1	0.5	583 423.4	303	3.4	2.0037 ± 0.0001	8.70 ± 0.01	0.73
N2	10	575.8 388.8	309.8	3.6	2.0035 ± 0.0001	8.41 ± 0.01	0.83
N3	17	583.2	315.4	4.0	2.0034 ± 0.0001	8.33 ± 0.02	0.84
A1	1	390	322				1.00
A2	3	485					1.00
A3	5	493					0.83
A4	7	520			2.0050 ± 0.0005	8.49 ± 0.01	1.00
B1	5 (ZnS/glass)	472					
B2	ZnS: Mn^{2+} bulk powders	581	350.4		2.0027 ± 0.0001	6.99 ± 0.01	1.00

different particle sizes and ZnS: Mn^{2+} bulk powders/glass is shown in Figures 1 and 2. The sizes of ZnS: Mn^{2+} nanocrystals/glass are 3.4, 3.6, and 4.0 nm in diameter, corresponding to the samples N1, N2, and N3 as listed in Table I. In general, Mn^{2+} ions substitute Zn^{2+} ions in ZnS: Mn^{2+} nanocrystals. Excitation and emission processes of Mn^{2+} ions in ZnS: Mn^{2+} nanocrystals/glass are carried out with a fluorometer. A 300-nm light from a xenon lamp is used to excite the sample through a band-to-band excitation of ZnS, followed by either a radiative transition giving rise to luminescence or by an energy transfer from ZnS to Mn^{2+} ions. The excited Mn^{2+} ions as luminescence centers in ZnS: Mn^{2+} gives rise to an orange emission at about 581 nm that is assigned to the $^4T_1$–$^6A_1$ transition of Mn^{2+} ions. In other words, the 581-nm emission originates from Mn^{2+} ions through the energy transfer from the sp^3-hybrid orbital of ZnS to the d electrons of Mn^{2+}. This is a common feature for Mn^{2+} ions substituting Zn^{2+} ions in ZnS: Mn^{2+} using a band–band excitation.

Examination of the PL spectra in Figure 1 reveals that the $^4T_1$–$^6A_1$ emission bands in nanocrystals are broadened by about 20 to 30 nm compared with ZnS: Mn^{2+} bulk materials. The spectral broadening may be due to the following reasons: (1) size distribution of ZnS: Mn^{2+} nanoparticles instead of monodispersion, (2) Mn^{2+} ions residing at different sites, e.g., substituting zinc and occupying the space between Zn and S ions either inside or outside nanocrystals, and (3) enhancement of the electron–phonon couple in ZnS: Mn^{2+} nanoparticles due to size confinement. In addition, the ($^4T_2$ or $^4A_1$)–$^6A_1$ transition from Mn^{2+} ions is a possible reason for the spectral broadening. Spectral shifting can be found in Figure 1

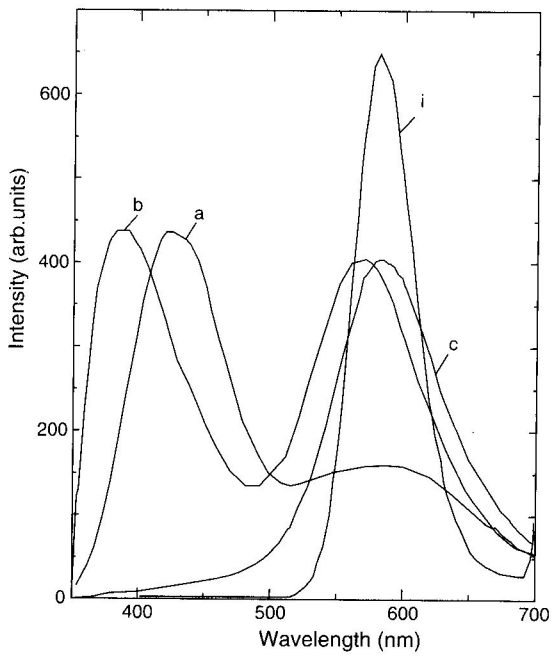

Fig. 1. Comparison of emission spectra of ZnS: Mn^{2+} /glasses at different nanocrystal sizes: (a): 3.4 nm (N1), (b): 3.6 nm (N2), (c): 4.0 nm (N3) and (i): bulk material (B2). The curve (i) should be multiplied by 25.

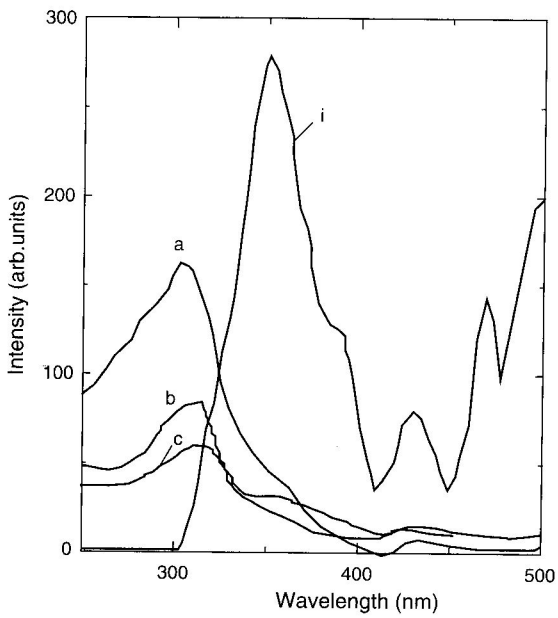

Fig. 2. Comparison of excitation spectra of ZnS: Mn^{2+} /glasses at different nanocrystal sizes: (a): 3.4 nm (N1), (b): 3.6 nm (N2), (c): 4.0 nm (N3) and (i): bulk material (B2). The curve (i) should be multiplied by 10.

RESEARCH ARTICLE

by examining the 581-nm emission from the $^4T_1$–$^6A_1$ transition. The $^4T_1$–$^6A_1$ emission peak of ZnS: Mn^{2+} nanocrystals with sizes of 3.4 and 4.0 nm in diameter is found to have a red shift to 583 nm compared with 581 nm for the bulk sample. This is understandable by looking at the previous results, for example, the decrement of the Mn–S separation with decreasing the nanocrystal size[6] and the reduction of the $^6A_1 \rightarrow {}^4T_1$ transition probability when the metal ion ligand increases due to the substitution of Zn with Mn ions.[7] In this paper, we do not have a good explanation for the abnormal shifting to 575 nm rather than to 583 nm in the PL spectra of 3.6-nm ZnS: Mn^{2+} nanocrystals/glass shown in Figure 1 and further experimental investigation and analysis are needed in order to understand the abnormal shifting in ZnS: Mn^{2+} nanocrystals/glass with a size of 3.6 nm.

ZnS: Mn^{2+} nanocrystals/glass with a size of 3.4 nm exhibit an emission at 423.4 nm which is identified as "self-activated" (SA) emission caused by the Zn vacancies (V_{Zn}) in the lattice of ZnS consistent with the result reported.[2] With increasing Mn^{2+} concentration, SA luminescence disappears in emission spectra as seen in Figures 1 and 3. The orange emission from the $^4T_1$–$^6A_1$ transition of Mn^{2+} is not observed in the samples A1, A2, and A3 corresponding to 1%, 3%, and 5% resulting from either weak *sp-d* electron state mixing or no energy transfer between the ZnS matrices and the Mn^{2+} ions. It is inferred that some Mn^{2+} ions may not fill up the Zn^{2+} sites, but occupy the interstitial sites, denoted by $(Mn^{2+})_{int}$. As calcining temperature increases over 950 °C, ZnS displays a mixture of cubic and hexagonal phases.[8] The cubic phase of ZnS possesses a lattice constant (σ) of 0.541 nm. However, the hexagonal phase has $\sigma =$ 0.381 nm in the direction perpendicular to the c axis and $\sigma = 0.623$ nm along the c axis. Since the ionic radius of Mn^{2+} is 0.091 nm, Mn^{2+} may reside, even in the mixing phase, at sites either among molecules of ZnS or between ZnS and glass. The latter leads to a formation of $(Mn^{2+})_{int}$ configuration, showing the emission spectra in Figure 3. In particular, Mn ions located at the sites around ZnS: Mn^{2+}, or Mn-activated (outside) nanocrystals in solution[2,9] give an example for $(Mn^{2+})_{int}$. Therefore, two types of centers associated with the occupation of manganese ions at different locations of either substitutional or interstitial sites can spectrally be identified.

In addition, the sizes of the nanocrystals in Table I for the current experiment were obtained by calculating the blue shift in PLE spectra using Brus' method,[10] assuming that the effective mass of an electron and a hole are 0.42 m_e and 0.61 m_e, respectively, with a dielectric constant of 8.0 in ZnS.

3.2. EPR spectra

The EPR technique is very sensitive to the configuration surroundings of an ion in a solid and often used to identify

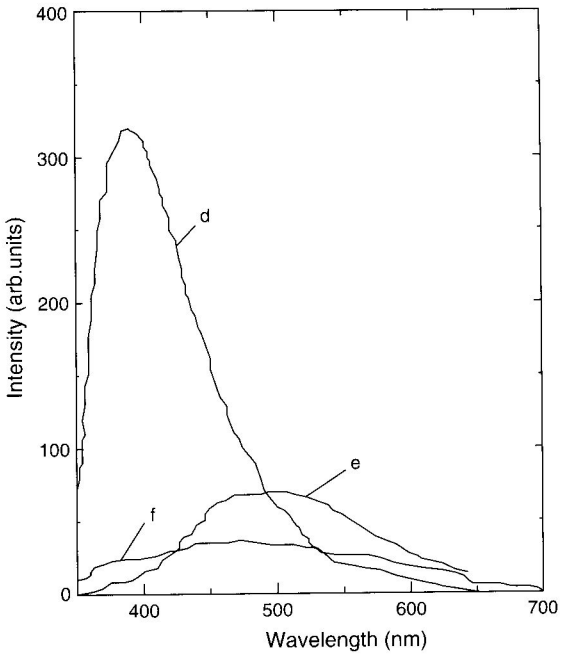

Fig. 3. Emission spectra for the samples with different weight ratios of ZnS: Mn^{2+} to the glass. (d): A1–1%, (e): A2–3%, and (f): A3–5%.

dopants at different occupying sites. Manganese ions in ZnS: Mn^{2+} can be identified at different sites of occupation, such as substitutional and interstitial site denoted, respectively, as $(Mn^{2+})_{sub}$ and $(Mn^{2+})_{int}$, or even manganese aggregates (clusters) can be identified. $(Mn^{2+})_{sub}$ and $(Mn^{2+})_{int}$ are also defined as Type-I and Type-II sites of Mn.[5] To confirm the spectral results obtained in the PL measurements, EPR experiment was carried out with the same samples as ones used for the PL experiments. Spectral features associated with three types of sites of

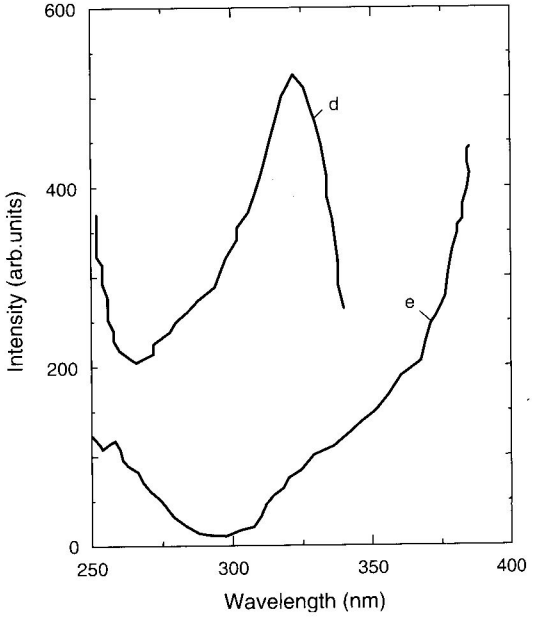

Fig. 4. Excitation spectra for samples A1 (d) and A2 (e).

RESEARCH ARTICLE

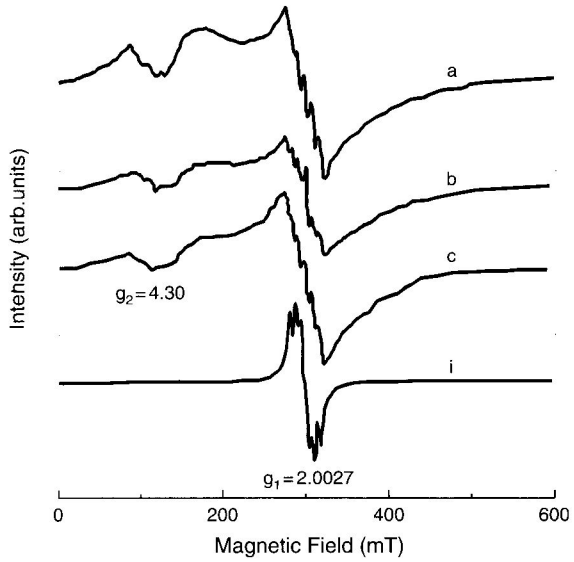

Fig. 5. EPR spectra of ZnS: Mn^{2+}/glasses at different nanocrystallite sizes. (a): 3.4 nm for N1, (b): 3.6 nm for N2, (c): 4.0 nm for N3 and (i): bulk material for B2.

$(Mn^{2+})_{sub}$, $(Mn^{2+})_{int}$, and Mn clusters were found in EPR measurements, consistent with the results obtained in the PL spectra.

Figures 5 and 6 represent the EPR spectra for all samples listed in Table I. The EPR spectra show a common feature in the signal traces consisting of three components. The first component is a hyperfine sextet spectrum which is superposed on a broad background centered at about $g_1 = 2.00$. The six-line spectrum characterizes Mn^{2+} occupying Zn^{2+} sites, i.e., $(Mn^{2+})_{sub}$, is known as Type-II sites of Mn in a glass matrix.[5] Different signal intensities in the hyperfine sextet indicate an asymmetry of the Mn ions in ZnS. This symmetry is lower than a cubic phase and thus a hexagonal phase is dominant in our samples. The second component is the broad background attributed to the strong dipole–dipole exchange interaction among

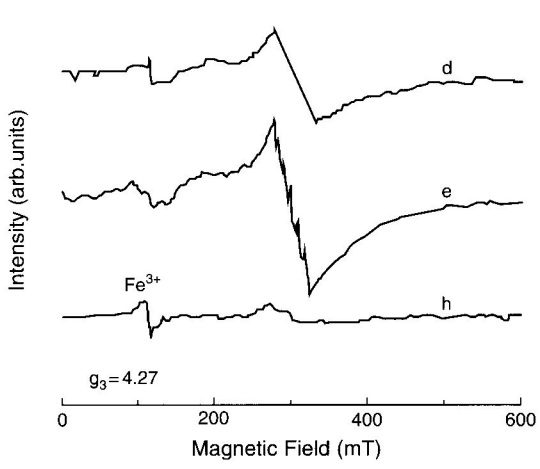

Fig. 6. EPR spectra for the samples with different weight ratios of ZnS: Mn^{2+} to the glass. (d): A1–1% and (e): A2–3%. ZnS/glasses (h) is drawn as a reference for comparison.

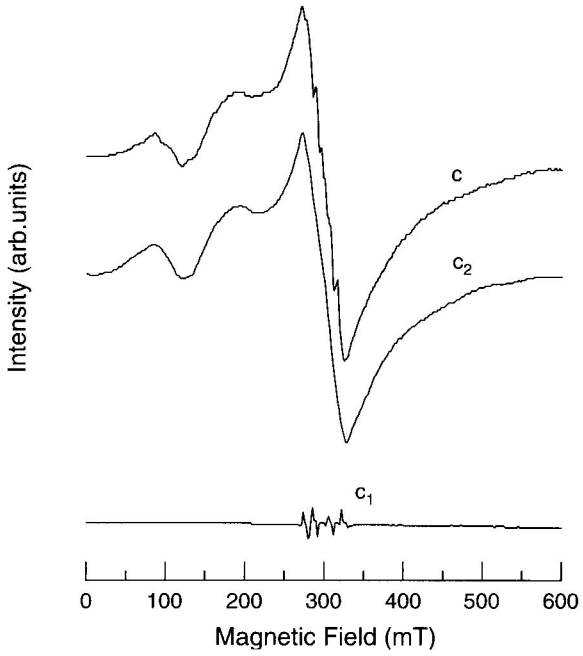

Fig. 7. EPR spectrum of Figure 5(c) for N3 with a size of 4.0 nm in diameter is decomposed into two components of $C = C_1 + C_2$.

Mn ions in clusters. To distinguish the contributions of $(Mn^{2+})_{sub}$ from Mn clusters in the EPR signals, the curve C in Figure 5 was decomposed into two components denoted by the curve C_1 and C_2 as shown in Figure 7. Curve C_1 is the six-line spectrum representing the contribution from $(Mn^{2+})_{sub}$, and the broad spectrum C_2, is assigned to Mn clusters. Therefore, Mn clusters produces a more contribution over the substitutional Mn. The third spectrum is the band centering at $g_2 = 4.3$ which was assigned to $(Mn^{2+})_{int}$, consistent with the EPR signals of Fe^{3+} with $3d^5$ electron configuration observed at $g_3 = 4.27$ (Fig. 6(h)).[11]

Parameters A, B, and C are hereafter introduced for an analysis of EPR spectra. The amplitudes A, B, and C are related to the numbers of $(Mn^{2+})_{sub}$, Mn cluster and $(Mn^{2+})_{int}$, respectively, if A, B and C are defined as drawn in Figure 8 which represents a variation of A, B, and C in mm/g (mm: signal strength in EPR spectrum, g: mass) versus percentage of ZnS: Mn^{2+} in Pyrex glasses. A, B, and C exhibit a minor change for all samples when the composition of ZnS: Mn^{2+} is below 10%. The amplitude A for nanocrystals of N1, N2 and N3 is found to be greater than that of the others in Figure 8, corresponding to the strong $^4T_1$–$^6A_1$ emission of $(Mn^{2+})_{sub}$ (also see Figure 1(a–c)). The ratio of A_{up}/A_{down} given in Table I reflects a spectral symmetry.[4] The ^4G–^6S transition of Mn^{2+} is spin forbidden ($\Delta S = 1$). The perturbation of the crystal-field makes the $^4T_1$–$^6A_1$ transition partially allowed. The EPR signals for samples N1, N2, and N3 have shown a stronger symmetry breaking due to $A_{up}/A_{down} < 1$ than the other samples having $A_{up}/A_{down} = 1$, consistent with the strong $^4T_1$–$^6A_1$ emission recorded in Figure 1. The EPR spectrum

RESEARCH ARTICLE

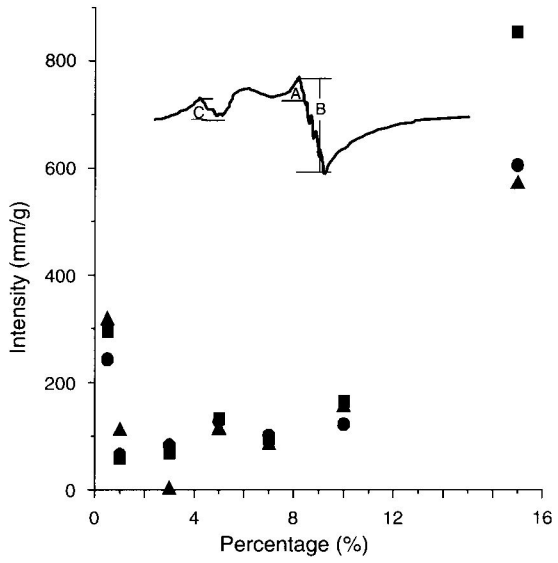

Fig. 8. Intensity of EPR signals (mm/g) versus percentage of ZnS: Mn^{2+} in Pyrex glasses, •—A; ■—B (÷6); ▲—C.

for bulk powders with $A_{up}/A_{down} = 1$ exhibits a symmetric shape due to much more Mn^{2+} luminescence centers in the bulk materials than in the nanocrystals, leading to the strong $^4T_1$–$^6A_1$ transition. The amplitude B of Mn cluster (divided by six in Fig. 8) is found to be enhanced with increasing concentrations of Mn ions. The amplitudes B are apparently greater than A and C in all samples. It can be concluded that most of Mn ions are aggregated, leading to forming Mn clusters during calcining.

The spin Hamiltonian for Mn^{2+} ions ($S = 5/2$, $I = 5/2$) in the nanocrystals is given[12, 13] by,

$$H = H_{Zee} + H_{HFS} + H_{cf} + H_{FS} \quad (1)$$

$H_{Zee} = g\beta\mathbf{H} \cdot \mathbf{S}$ describes the Zeeman energy having a typical magnitude of $0 \sim 1$ cm^{-1}. $H_{HFS} = A\mathbf{S} \cdot \mathbf{I}$ ($0 \sim 10^{-2}$ cm^{-1}) represents the hyperfine structure produced by the interaction of nuclear spins with an unpaired electron. $H_{cf} = (1/6)a(S_x^4 + S_6^4 + S_z^4)$ involves a high spin ($S \geq 3/2$) for the cubic-field splitting which was already observed in oriented single crystals. The last term $H_{FS} = D[S_z^2 - (1/3)S(S+1)]$ denotes the fine structure splitting resulting from the spin–spin interaction. The fine structure H_{FS} has a typical value of $0 \sim 1$ cm^{-1}.

The EPR trace (i) in Figure 5 is obtained from ZnS: Mn^{2+} powders having a zinc blende structure. The tetrahedral symmetry as shown in the six HFS lines represents the isotropic fine structure transition from $|1/2, m\rangle$ to $|-1/2, m\rangle$. $g_\parallel = 2.0027 \pm 0.0002$ and $|A| = 6.99 \pm 0.01$ mT are determined from the data in Figure 5. In general, the symmetry of EPR signal traces of the ions in a solid reflects the symmetry associated with the surrounding microenvironment of the ions. From Figure 5 that the symmetry of Mn^{2+} EPR spectra in nanocrystals (traces *a*, *b*, and *c*) is significantly lower than that of bulk powders (trace *i*), the reason for some forbidden optical transitions in bulk materials become partially allowed in nanomaterials. When the diameters of the nanocrystals decrease from 4 to 3.4 nm, $g_\parallel$ factors increase from 2.0034 ± 0.0002 to 2.0037 ± 0.0001 and HFS $|A|$ increase from 8.33 ± 0.02 to 8.70 ± 0.01 mT. One reason for the *g*-factor shift is the changes of the discrete energy levels of ZnS matrices due to a coupling between the *s-p* states of ZnS and the *d* states of Mn ions caused by quantum confinement. The other possible reason is that the surface/volume ratio increases as the size decreases and the surface states (dangling bounds, defect sites, etc.)

4. CONCLUSION

EPR and optical measurements reveal that Manganese ions in ZnS: Mn^{2+} nanocrystals dispersed Pyrex glasses form three types of centers residing at three different microenvironments, identified as $(Mn^{2+})_{sub}$, $(Mn^{2+})_{int}$ and Mn cluster. A change in the $g_\parallel$ factor and HFS constant with decreasing nanocrystal sizes may result from quantum confinement effects and surface states.

Acknowledgments: The authors J. Y. Liu and C. X. Liu thank the National Foundation of Natural Sciences of China and Laboratory of Excited State Processes for supporting the project.

References and Notes

1. R. Bhargava, D. Gallagher, X. Hong, and A. Nurmikko, *Phys. Rev. Lett.* 72, 416 (**1994**).
2. K. Sooklal, B. Cullum, S. Angel, and C. Murphy, *J. Phys. Chem.* 100, 4551 (**1996**).
3. J. Yu, H. Liu, Y. Wang, F. Fernandez, W. Jia, L. Sun, C. Jin, D. Li, J. Liu, and S. Huang, *Opt. Lett.* 22, 913 (**1997**).
4. J. Liu, C. Liu, W. Xu, and D. Li, *Science in China* 42, 388 (**1999**).
5. D. Griscom and R. Griscom, *J. Chem. Phys.* 47, 2711 (**1967**).
6. Y. L. Soo, Z. H. Ming, S. W. Huang, Y. H. Kao, R. Bhaargava, and D. Gallagher, *Phys. Rev.* B50, 7602 (**1994**).
7. F. Rodriguez and M. Moreno, *J. Chem. Phys.* 84, 692 (**1986**).
8. W. Lu, M. Xu, and W. Huang, *Chin. J. Lumin.* 13, 355 (**1992**).
9. J. Gomez Sal, F. Rodriguez, and M. Moreno, *J. Tholence, Phys. Rev.* B37, 454 (**1988**).
10. L. Brus, *J. Phys. Chem.* 80, 4403 (**1984**).
11. T. Castner, G. Newell, W. Holton, and C. Slichter, *J. Chem. Phys.* 32, 668 (**1960**).
12. T. Kennedy, E. Glaser, P. Klein, and R. Bhargava, *Phys. Rev.* B52, R14356 (**1995**).
13. C. Poole, in *Electron Spin Resonance*, Wilely, New York (**1983**), p. 8.
14. E. Simanek and K. Muller, *J. Phys. Chem. Solids* 31, 1027 (**1970**).

Received: 16 December 2004. Accepted: 7 March 2005.